ATLAS Internal Note
October 26, 2001

First straw straightness measurements on a 4-plane end-cap ATLAS TRT wheel

A. Lucotte[1,2)], S. Kovalenko[3)], V.A. Mitsou[1,4)], S. Mouraviev[1,5)], A. Nadtotchi[3)]

ATL-INDET-2002-007
15/04/2002

Abstract

This document reports the first results and their interpretation of the straw straightness measurements that have been performed on the first 4-plane end-cap prototype of the ATLAS TRT.

Section 2 presents the experimental setup used for the measurements, as well as a review of the data sample used to perform this study. It also provides a description of the method used to assess straw straightness, which is based on the measurements of the maximal gas gain deviation ("straw eccentricity") seen along the straw. Section 3 reports the results of straw straightness for the 4-plane module, including corrections due to the gas flow. The effect of energy resolution degradation is also explained and results in terms of wire offset are reported. In Section 4, the straw bending due to an applied lateral deformation is measured, and finally Section 5 reviews the conclusions.

[1)] CERN, EP Division, CH-1211 Geneva 23, Switzerland
[2)] now at Institut des Sciences Nucléaires, IN2P3-CNRS, Universite de Grenoble 1, Grenoble, France
[3)] Petersburg Nuclear Physics Institute, Gatchina, St. Petersburg, Russia
[4)] University of Athens, Physics Department, Nuclear and Particle Physics Section, Panepistimioupolis, GR-157 84 Athens, Greece
[5)] P.N. Lebedev Institute of Physics, Moscow, Russia

Contents

1 Introduction

The mechanical accuracy of the wire position inside the straw and the straw straightness are the most stringent requirements set by the need for stable and robust operation of the ATLAS TRT over many years running at the LHC ([1] p. 622). More specifically, it has been shown that over the chosen straw gas gain range, stable and robust operation of the straws at the LHC can be achieved, provided that the wire offset is less than 300 μm along the full length of the straw.

The straw straightness can be assessed via the determination of the straw eccentricity parameter. It is due to two main factors: either the wire inside the straw is not properly centred in the wire guides or the straw wall itself is bent. In both cases, the effective electrical field seen by electrons drifting towards the anode wire is distorted, thus affecting the gas gain and the energy resolution of the straw chamber. These effects have been studied in Ref. [2], where distortions of the radial symmetry of the electrical field inside a straw tube have been simulated in great detail using `GARFIELD` and `MAGBOLTZ`. Comparison of those models with individual straw measurements helped characterize the effects of a wire offset on the signal amplification as well as on the energy resolution.

The purpose of the present study is to perform similar measurements on a large scale for the 3 072 straws of the first 4-layer end-cap wheel, in order to identify and isolate various possible sources of gas gain variation that could occur during normal running conditions. The experience acquired through this process is fed to the final design of the Wheel Test Station (WTS) [4]. This is a device which will be used for the test of all end-cap TRT wheels during the production phase. Apart from those issues, an interpretation of the measured eccentricity in terms of wire offset is provided for the full statistics of this module.

2 Experimental setup and method of the measurement

2.1 Experimental setup

Two radioactive ^{55}Fe sources of 185 MBq activity, embedded in a polycarbonate block, are used to irradiate the straws with 5.9 keV X-rays through a 4 mm-wide collimation slit, perpendicular to the straw axis. For each straw, signal amplitude is recorded at three different positions[1] of the source, located at $L_1 = 15$ mm (inner), $L_2 = 180$ mm (centre), and $L_3 = 315$ mm (outer). The sources are then moved around the wheel to ensure a complete coverage of all 3 072 straws. A schematic view of the experimental setup used to test the first 4-plane module is shown in Fig. 1.

A schematic view of the wheel prototype tested is shown in Fig. 2. In this series of measurements, the wheel is positioned horizontally on a table, laying on metallic supports located at cells[2] 5A-5, 3C-4, 2B-1, 7B-6, 6B-4, and 5C-2. The gas distribution system

[1] The positions are measured with respect to the outer surface of the inner ring.

[2] The cells are numbered according to the web code (e.g. 5A) and the cell number within the web (1–6).

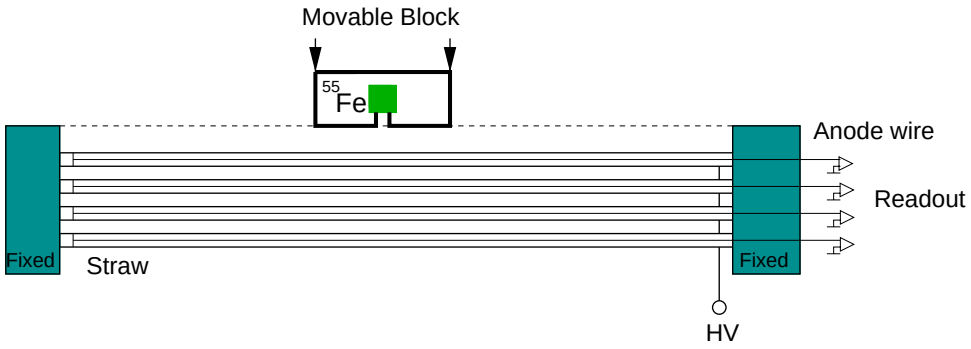

Figure 1: *Transverse view of the experimental setup for wire offset measurements on the first 4-plane end-cap wheel.*

used for these measurements is also displayed in Fig. 2. The active gas, $70\%\mathrm{Ar}+30\%\mathrm{CO}_2$, is flown into the wheel via five inlets located at the outer diameter (cells 2A-5, 7A-5, 6B-5, 3C-5, 4D-5), while flown out of the wheel via four gas outlets in the inner diameter of the wheel.

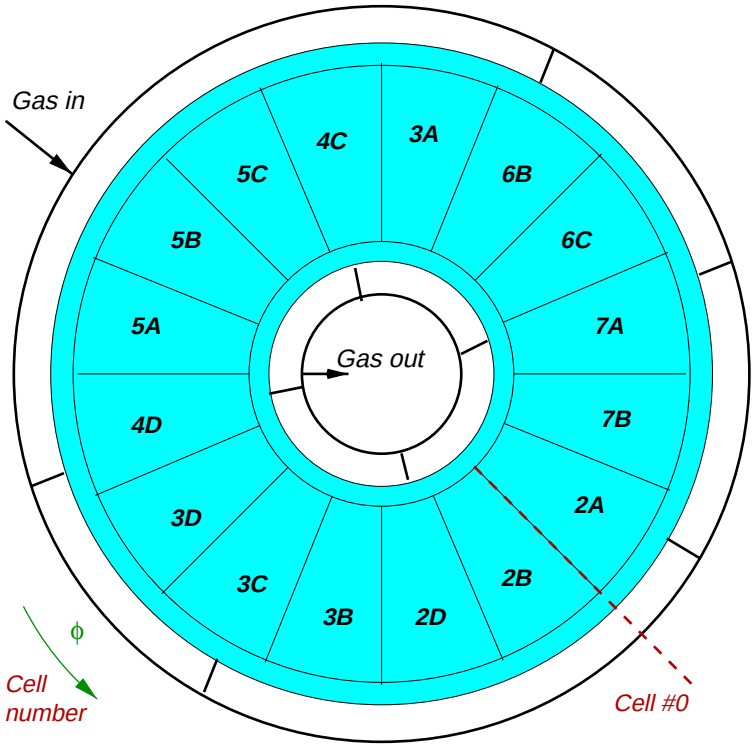

Figure 2: *Distribution of the gas inlets for the first 4-plane end-cap wheel. The inlets are located in cells 2A-5, 7A-5, 6B-5, 3C-5, and 4D-5. The supports are in cells 5A-5, 3C-4, 2B-1, 7B-6, 6B-4, and 5C-2. The equivalence of webs in terms of cell number is given in App. B.*

The 96 cells of 32-straws are readout through a FE board using two GASSIPLEX chips. Only two channels are readout simultaneously. Signals are sent to CROSS modules, where they are logically OR-ed for the trigger. More on the data acquisition system is described in Ref. [4].

2.2 Description of the method

2.2.1 Straw eccentricity parameter

At each point, the signal amplitude is determined from the main peak of the ^{55}Fe X-ray energy spectrum. Both the escape (2.7 keV) and the main (5.9 keV) peaks can be used to set the energy scale (conversion of ADC channels to keV) per straw. A typical spectrum is displayed in Fig. 3, where a threshold is set at $T = \langle \text{pedestal} \rangle + 8\langle \sigma_{\text{pedestal}} \rangle$ to avoid any significant contribution from the noise to the ^{55}Fe spectrum. The first peak corresponds to the escape peak, while the main peak is used to determine the signal amplitude. The relative position of the two peaks allows to perform a calibration of the data by using the natural shift between the two peaks: 5.9 keV−2.7 keV. A two-Gaussian fit is performed on each point of measurements, resulting in the determination the number of counts inside the peak, mean peak position and sigmas.

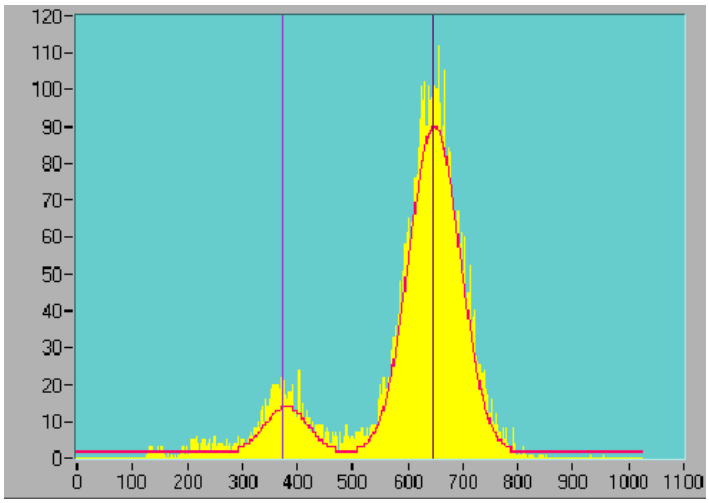

Figure 3: *Pedestal-subtracted* ^{55}Fe *spectrum as obtained at one point along the straw. A two-Gaussian fit (one for each peak) has been applied.*

Measurements are made for several source locations per straw and the average value, A_{avg}, is computed. At each point of measurement, a deviation from the average amplitude is observed, which is sensitive to the wire offset. The straw straightness then can be characterized by the "eccentricity" or "gas gain variation" parameter $\delta A/A$ [3]. This parameter is defined as the maximal gas gain variation observed along the straw,

$$\frac{\delta A}{A} \equiv \frac{A_{\text{max}} - A_{\text{min}}}{\text{A}_{\text{avg}}}, \tag{1}$$

where A_{max} (A_{min}) is the maximal (minimal) signal value recorded along the straw.

Figure 4 displays typical spectra observed at the centre of the straw for three different values of $\delta A/A$; for 1.0%, 2.9%, and 5.1%. They are simulated using the experimental determination of the signal mean peak positions, widths and sample sizes from recorded data. Note that the superposition of two Gaussians was used to fit the observed spectrum of the main peak, and also to produce the simulated spectrum as suggested in Ref. [2]. It is clear that as the $\delta A/A$ parameter increases, the peak position migrates to higher values and the peak becomes wider and asymmetric. The last point will be discussed in detail in Sec. 3.6.

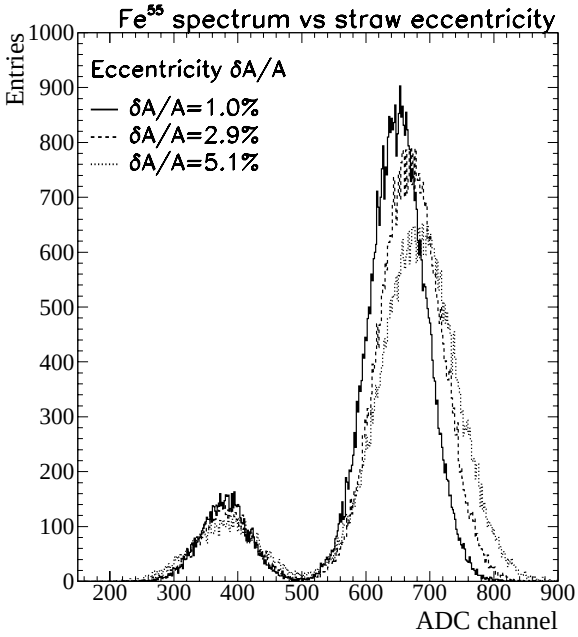

Figure 4: *Simulated* ^{55}Fe *spectra using experimental input: signal mean peak positions, widths and relative weights for escape and main peak are extracted from recorded data. Straws with various eccentricity values were used:* 1.0%, 2.9%, *and* 5.1%, *corresponding approximately to wire offsets of* 130 μm, 240 μm, *and* 310 μm, *respectively.*

It should be noted that the $\delta A/A$ parameter accounts only for the variation of the mean peak position of the 5.9 keV peak. Asymmetry and the high energy tail that appear in the case where there is a strong eccentricity have also to be monitored in order to understand the bias on the energy resolution. The precision of the eccentricity measurement is about 0.1%.

2.2.2 Straw eccentricity versus wire offset

The interpretation of the gas gain measurements in terms of wire offset makes use of the results of previous studies [2]. For a mixture of 76%Ar + 24%CO_2 (which resembles the one used for the straightness measurements), the gas gain variation as a function of the wire offset is shown in Fig. 5.

Wire offset	Gas gain variation
100 μm	0.7%
200 μm	2.45%
300 μm	4.8%
400 μm	8.2%

Table 1: *Experimentally obtained gas gain variations for different values of wire offset, measured with a gas mixture of* 76%Ar + 24%CO_2 *and a wire of* 30 μm *diameter [2].*

Typical values corresponding to a 100, 200, 300, and 400 μm wire offset are reported in Table 1. It can be seen that a 300 μm wire offset induces a local change in the amplitude of about 4.8%. This sets stringent constrains on the precision we need to achieve in order to identify bent straws, especially when the energy resolution is degraded.

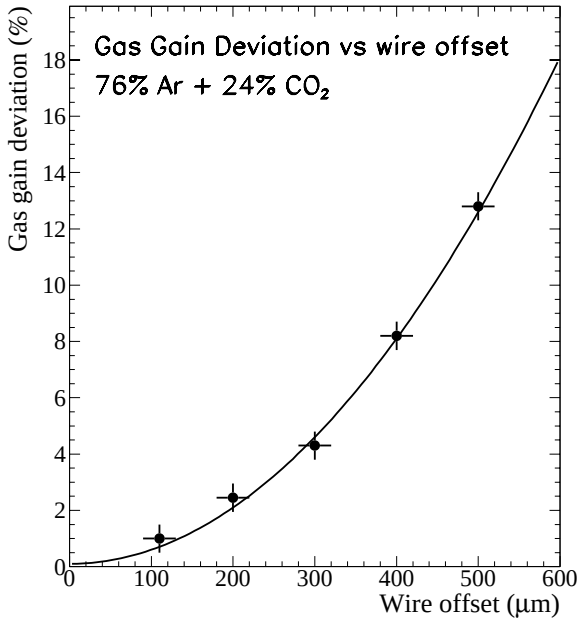

Figure 5: *Measured gas gain variation as a function of wire offset for a mixture of* $76\%\mathrm{Ar} + 24\%\mathrm{CO}_2$*, a wire of* 30 μm *diameter and a high voltage of* 1366 V *[2]. The experimental points have been fitted with a second-degree polynomial.*

2.3 Statistics and uniformity of the measurements

2.3.1 Statistics and parameter settings

A total of 96 cells of 32 straws each are readout. Among the 3 072 straws, 252 (8.2%) are found "dead" (no response). The distribution of the dead channels in the four layers is presented in Table 2. Dead channels are mostly found in layers 2 and 4 (77 in average) than in layers 1 and 3 (44 in average).

Layer	Number of dead channels
1	37 (4.8%)
2	75 (9.8%)
3	52 (6.8%)
4	79 (10.3%)
All	252 (8.2%)

Table 2: *Distribution of dead channels among the layers.*

A more detailed account of the dead channels, such as the ϕ-location and the per-cell distribution of them, is presented in App. A. Explanation of these distributions is also given. A total of 2 820 straws are thus remaining available for the analysis. The overall significant number (8.2%) of dead channels can be explained by two main reasons:

- Broken traces on the Kapton layer of the web (~ 220 cases). These channels are identified as containing broken traces, which is related to the high number of manipulations they have underwent during various tests (wire tension, high voltage, etc.).

- Presence of a mylar layer still covering the straw. Some of the dead channels may indicate the presence of a mylar layer on the internal surface of the straw. In this case, a channel may show a signal in one or two out of the three locations where spectrum is recorded when the mylar cover is only partially removed.

Data have been recorded during two distinct periods, separated by about 6 months. The first period takes place in May 1999, while the second extends from December 1999 to February 2000. It should be noted that this data is split into two sets because two distinct FE electronics cards (denoted as card A and card B) are used for these measurements. They have very different characteristics; the average signal amplification value of card A is about 10% higher than that of card B. During the first period, data are taken with a fixed gas flux (20 l/h) and composition (70%Ar + 30%CO_2). Throughout the second period, data with several gas compositions, gas flow and high voltage settings are recorded. Table 3 reviews these configurations together with their corresponding statistics.

Card	Gas mixture Ar/CO_2	Gas flow (l/h)	High voltage (V)	Number of straws/cells		
				Cells	Channels	Read-out
A	70/30	20	1400	25	800	746
B	70/30	20	1400	05	160	158
B	100/43	10	1330, 1400	18	576	470
B	100/43	40	1330	06	192	184
B	150/82	22	1400, 1430	05	160	152
B	155/80	22	1400–1420	25	800	754
B	150/75	22	1400–1430	12	384	356
Total	—	—	—	96	3 072	2 820

Table 3: *Electronics, gas mixture, gas flux, and high voltage settings used for the data taking. The number of straws corresponding to each setting is reported in the last column.*

2.3.2 Uniformity of the measurements

Data are recorded independently for each of the 96 cells. A typical duration of a 32-straw cell measurement is about 45 min. During this period, three spectra per straw are recorded with about 10 000 accumulated counts each. The reproducibility of an individual amplitude measurement is monitored throughout the second period, and found to be better than 0.2%.

The average signal amplitude, A_{avg}, per straw is used to cross-check the uniformity of the measurements. The only correction applied is the pedestal subtraction. Figure 6 shows the average amplitude as a function of the high voltage settings and for various gas flux values from 10 to 40 l/h. At fixed gas flow, we observe the expected sensitivity of the signal response as the high voltage is increased. Points corresponding to different Ar/CO_2 gas mixtures (150/82, 155/80, and 150/75) are shown on the same plot for the

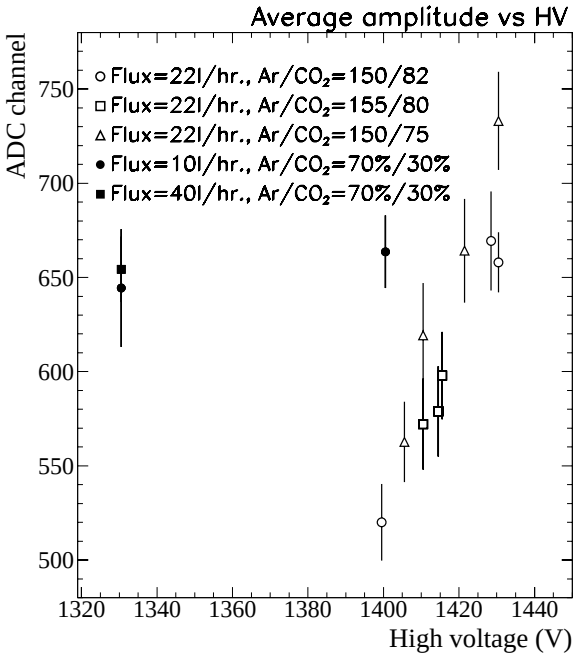

Figure 6: *Average signal amplitude (mean peak position) as a function of high voltage settings for various gas mixtures and flows. The error bars indicate the spread of the measurements.*

same range of variation. The error bars shown on the plot correspond to the spread of the signal amplitude measurements.

The uniformity of the measurements is examined by grouping all measurements into samples taken under the same conditions (i.e., high voltage, gas composition, gas flow) and looking at the individual signal (mean amplitude for the three positions along the straw) variation with respect to the average values computed per sample. Figure 7 displays the relative variation of the mean peak position measured per straw with respect to the average value as computed for each individual sample. For each straw, the difference is computed with respect to the signal averaged over a period where measurements are taken with the same high voltage, gas flow and gas composition settings.

The width of the overall distribution is found to be 3.7% as shown in Fig. 8. The corresponding variations for data samples taken in period 1 (card A) at 20 l/h, and in period 2 (card B) at 10, 22 and 40 l/h, are listed in Table 4. In all samples, the widths of the distributions are of the same order as the overall width (3.7%), hence the amplitude variations are due to parameters other than the gas flow value. No significant time-dependent effect is observed, as shown in Fig. 7, where variations are presented as a function of the straw index, thus following the time sequence of the measurements. The width of 3.7% may be explained by different factors:

- No calibration of the electronics has been performed, which may account for the channel-to-channel variation. This is the main source of pulse height variation.

- The precision on the gas composition setting is not accurate. The gas supply was often reset between complete measurements of cells, and this may have introduced a cell-to-cell variation.

- The high voltage supply unit produced a stable value only after about one hour of

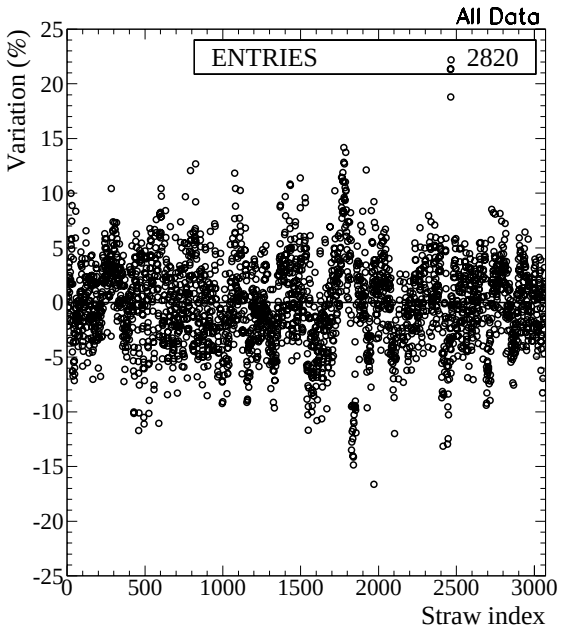

Figure 7: *Straw-by-straw mean amplitude variation (in %) with respect to the average value as a function of the straw index.*

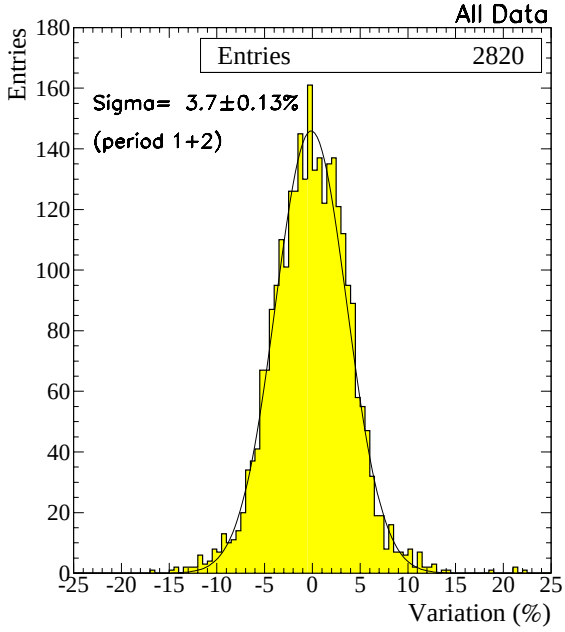

Figure 8: *Mean straw amplitude variation (in %) for all data recorded throughout periods 1 and 2.*

operation. During the first measurements of a shift, the high voltage was decreasing, and so did the signal amplitude.

- No monitoring of the temperature or pressure variation has been done, which can partially explain the cell-to-cell variation, since cell-measurements are typically separated by a few hours. This factor is known to affect significantly the amplitude by about 1% per degree. For this reason, a slow control system has been developed for the mass testing with the WTS.

Card	Gas flow (l/h)	σ of the variation (%)
B	10	3.1 ± 0.14
A	20	4.2 ± 0.13
B	22	3.9 ± 0.11
B	40	2.9 ± 0.2
Total	—	3.7 ± 0.13

Table 4: *σ of the amplitude variation for data samples obtained with the same gas flow value and electronics.*

It is worth noting that, in order to minimize the influence of environmental parameters during each period of data taking, pulse heights are recorded straw by straw at three locations, moving the source back to the first point for the next straw. Hence, the afore-

mentioned source of amplitude change does not affect significantly the recorded amplitude variation along the straw.

2.3.3 Straw shape

During the straightness measurements, it became evident that in many cases the maximum amplitude for a bent straw was not observed at its centre, but between the three irradiation points, as shown in Fig. 9. Hence, more points along the straw were needed in order to obtain a clear view of the straw shape. Since the presented measurements are performed manually, a possible increase of the number of irradiation points to more that three would increase substantially the time and effort to test all 3 072 straws. For the WTS, however, e.g., doubling the number of source positions would be a rather easy to achieve task.

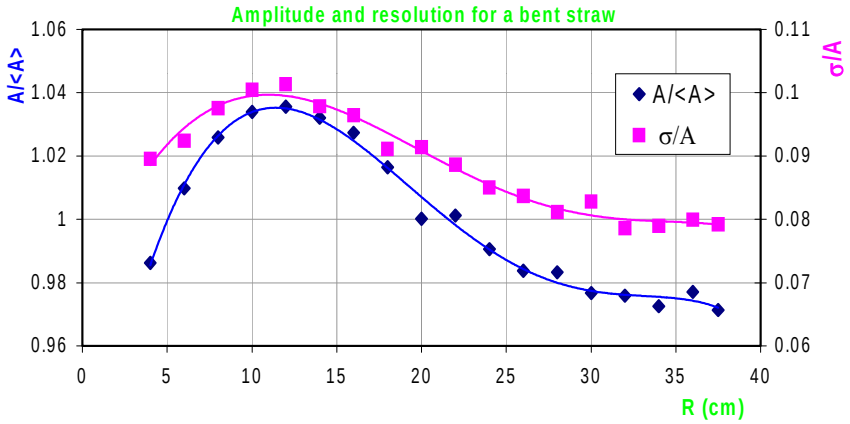

Figure 9: *Relative amplitude and corresponding resolution measured along a bent straw. The maximum is observed near the outer radius and not at the centre.*

3 Results from straw straightness measurements

Gas gain variation may be induced by to several factors. In the following, the overall gas gain deviation $\delta A/A$ per straw, as defined in the previous subsection, is first derived for all straws from the first module. Part of this deviation seems to be due to an effect related to the gas flow. This effect is described and gas gain measurements are corrected for it.

3.1 Gas gain variation measurements

All successfully readout (2 820) straws are irradiated in three points and the corresponding peak positions and ADC pedestals are recorded. Signal amplitude values are corrected for the pedestal before calculating the gas gain variation. Figure 10 displays the maximal gas gain variation per straw for the full wheel. About 95% of the straws have variations below or equal to 6%. Figure 11 shows the same variable, but presents the contribution from the different layers. It is clear that layer 1 (on the top of the wheel) straws have

undergone deformations that are not seen in the three others. This is expected since layer 1 underwent some mechanical deformations during the gluing of the straw plane to the rings. This effect was eliminated for layers 2, 3 and 4. Indeed, this is extracted from the numbers found for these three layers: more than 93% of the straws see less than a 5% variation, in contrast to the corresponding 88% for layer 1.

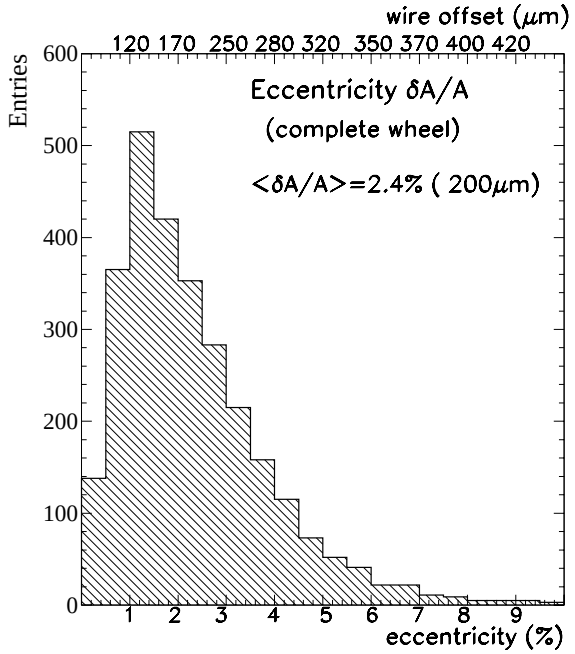

Figure 10: *Maximal gas gain variation for all straws of the wheel.*

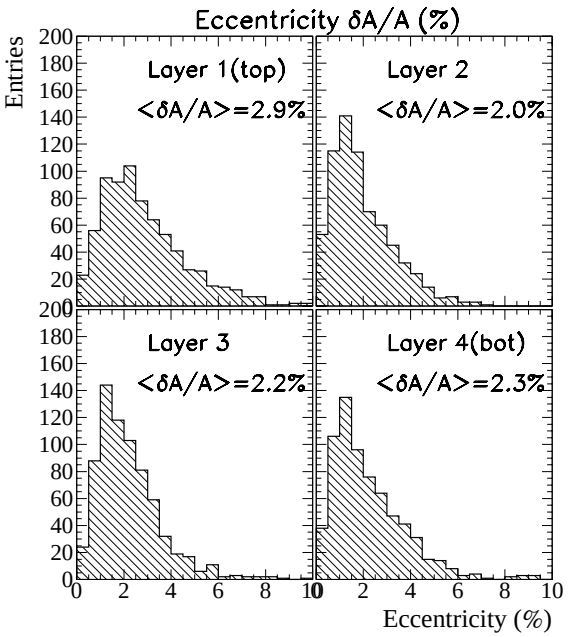

Figure 11: *Maximal gas gain variation for straws of each layer.*

3.2 Gas gain variation versus ϕ

On top of individual straw eccentricity, any non-uniformity in the gas distribution, or any mechanical deformation applied on a part of the wheel could give a rise to deviations in the $\delta A/A$ seen in a larger scale; typically a few cell-size. These two effects are investigated here.

Figures 12, 13, 14 and 15 display the measured $\delta A/A$ parameter in each of the four quarters of the wheel, as a function of ϕ expressed in straw index from 1 ($\phi = 0°$) to 768 ($\phi = 360°$) for layers 2, 3 and 4. Layer 1 is not displayed because it is already known that its straws have been deformed during installation. The locations of the gas inlets, as well as the supports (pedestals) on which the wheel is horizontally positioned, is also detailed on the plots.

A rather good uniformity in gas gain deviation is seen as a function of ϕ, the latter being denoted in terms of straw index per layer (768 straws per 360°). Some "bumps" are seen in the following regions:

- Straws 15–25 (cell 2), where a one-cell-sized bump is seen. This cell is not located

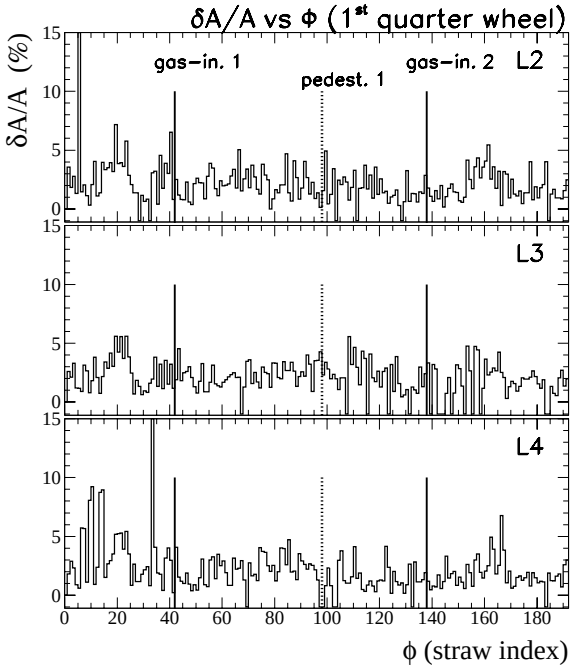

Figure 12: *Measured eccentricity $\delta A/A$ as a function of ϕ in the* 1^{st} *quarter of the wheel.*

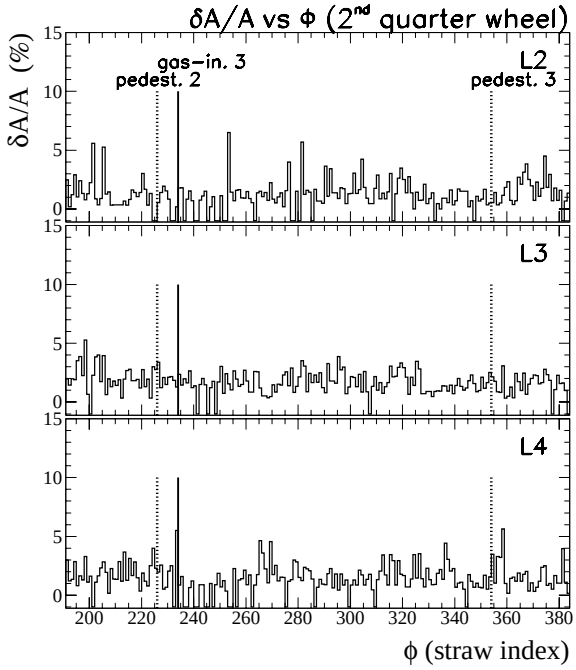

Figure 13: *Measured eccentricity $\delta A/A$ as a function of ϕ in the* 2^{nd} *quarter of the wheel.*

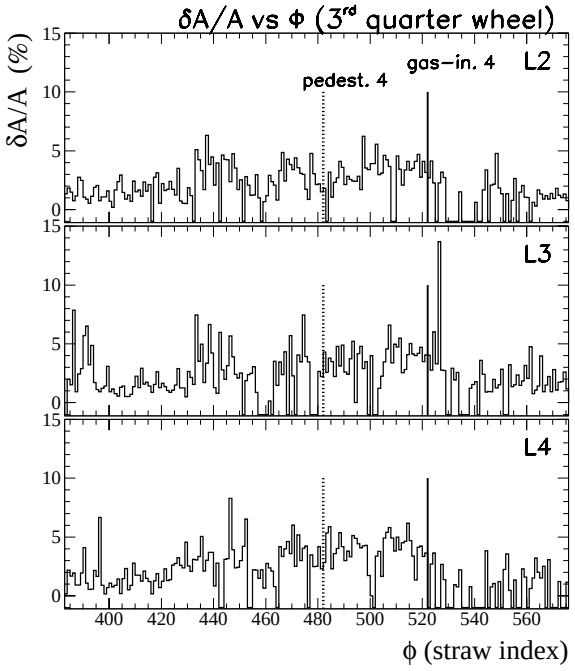

Figure 14: *Measured eccentricity $\delta A/A$ as a function of ϕ in the* 3^{rd} *quarter of the wheel.*

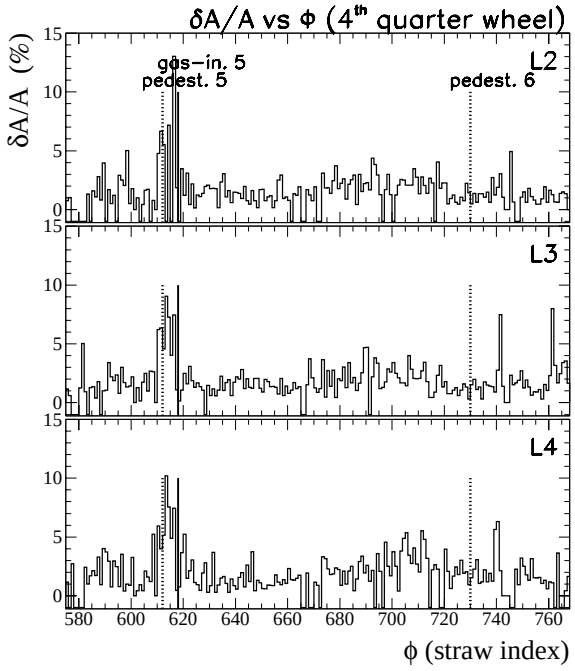

Figure 15: *Measured eccentricity $\delta A/A$ as a function of ϕ in the* 4^{th} *quarter of the wheel.*

at or near a support. However, the presence of this bump is compatible with fluctuations, and only 2 straws are found to have $\delta A/A > 5\%$.

- Straws 440–520 (cells 55–65), which show a $\delta A/A$ value significantly higher than in the neighboring cells. Pedestal 4 is located almost in the centre of this large area (37°), but does not seem to be related to this deviation, since no similar deviation is observed at the other pedestals. It should be noted however that very few straws are found with $\delta A/A > 5\%$.

- Straws 608–616 (cells 76–77), where a high bump is seen. This place corresponds to the region where the wheel is supported by pedestal 5. The sharpness of the peak excludes the possibility of a wheel deformation (in this case the effect would extend to several cells). This rise in eccentricity was eliminated when gas slope correction was applied (see next section).

It should be noted that measurements were repeated for cell 32, as well as for cells 70, 71 and 76, and no discrepancy with previous measurements was found. The observed patterns do not imply any serious deformation pattern and the cases with eccentricity is higher than 5% are rather isolated.

3.3 Gas gain variation due to gas flow

Gas gain decrease at the 1% level is observed when we measure signal amplitudes from the outer part of the ring inwards along the straw, i.e. in the direction of the gas flow. This can be clearly seen in Fig. 16, which shows the slope resulting from a linear fit versus $\delta A/A$ computed per straw. The slope values are determined by fitting the three amplitude points (outer-centre-inner) to a straight line. Clearly, a strong correlation is seen between these two variables, as expected. However the sign of this effect is negative in more than 95% cases, showing a signal amplitude decrease as we move from the outer part of the wheel inwards along a straw. Given the relatively poor resolution of the amplitude measurements (0.1%), no more sophisticated fit is considered in the following.

The same distribution of the eccentricity versus the slope is shown in Fig. 17, after applying a global correction to the amplitude values. This method and its effect on the eccentricity measurements is discussed in the next section. In this plot, it is clear that after the correction there is no preferable sign for the slope.

The results of a global fit to straws are presented in Fig. 18 for straws from layers 2, 3 and 4 for a gas flow of 22 l/h. The slopes obtained result in a mean value of $\alpha_{\text{flow}} = -0.78\%/(30\,\text{cm})$. No significant discrepancy is observed among the layers, where variations are found to range between -1.08% to -0.56% over a length of $L_3 - L_1 = 30$ cm.

This measurement is repeated for a gas flow of 10 l/h with a smaller statistical sample. Summing over all three layers (2, 3 and 4) result in an overall slope of $\alpha_{\text{flow}} = -1.24\%/(30\,\text{cm})$. The corresponding distribution is shown in Fig. 19. A comparison between the two slope distributions seems to show a dependence on the gas flow. The higher the gas flow, the lower is the decrease of gas gain along the straw.

As explained in App. C, this effect is due to the large permeability of the straw walls to CO_2 and O_2 molecules, which diffuse inside the straw. The diffusion of CO_2 outwards increases the gas gain, but the penetration of O_2 decreases it substantially, and the latter effect dominates. During the normal operation of the TRT in ATLAS, the straws will be closed in a CO_2 envelope, so this effect will not interfere with the detector performance.

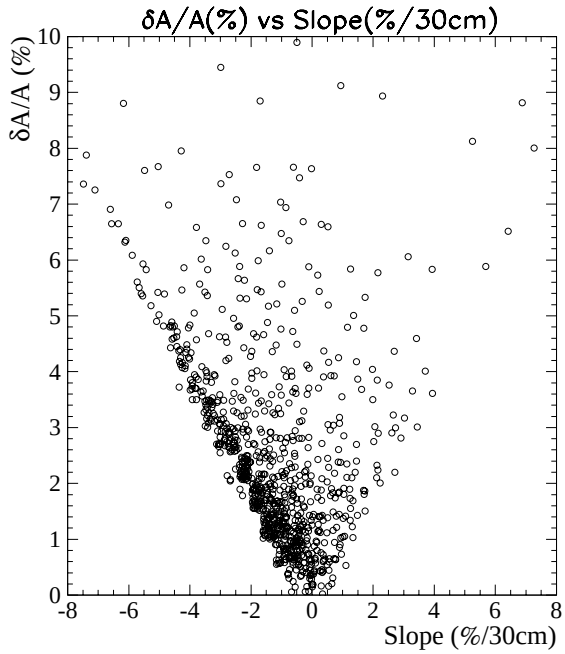

Figure 16: *Gas gain variation, $\delta A/A$, versus slope of gas gain for all 2 820 straws.*

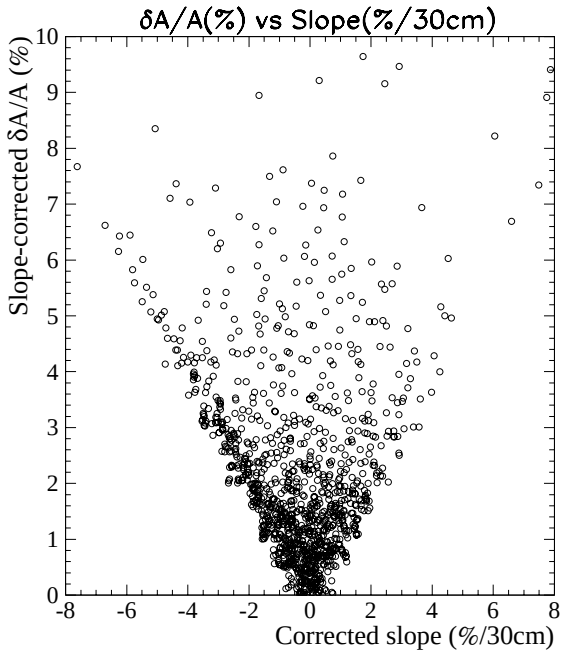

Figure 17: *Slope-corrected gas gain variation, $\delta A/A$, versus corresponding slope of gas gain for all 2 820 straws.*

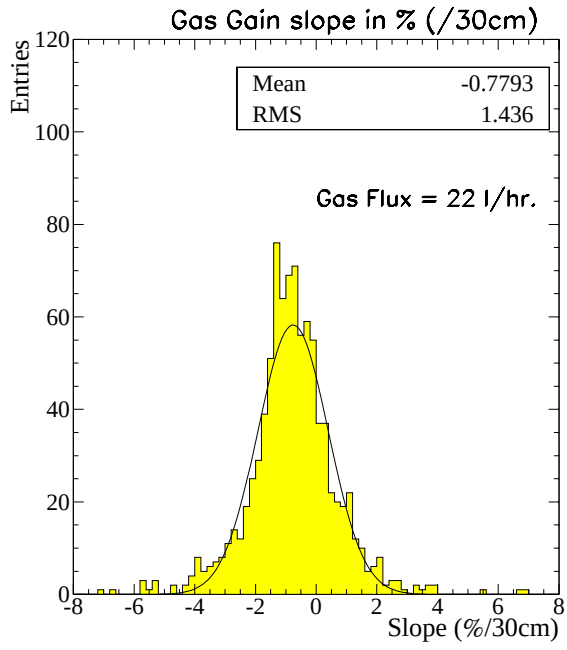

Figure 18: *Slope of gas gain for a flow of* 22 l/h *and for layers 2, 3 and 4.*

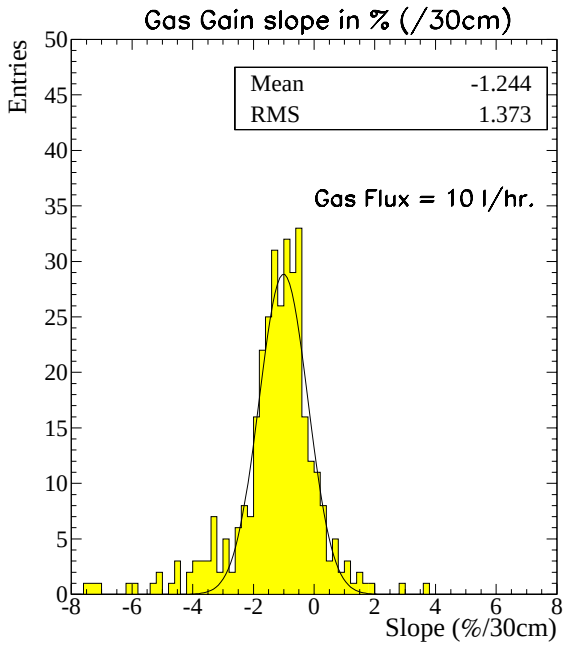

Figure 19: *Slope of gas gain for a flow of* 10 l/h *and for layers 2, 3 and 4.*

However, the wheel testing with the WTS will take place in the atmosphere, so its effect on the interpretation of the gas gain measurements was studied exclusively.

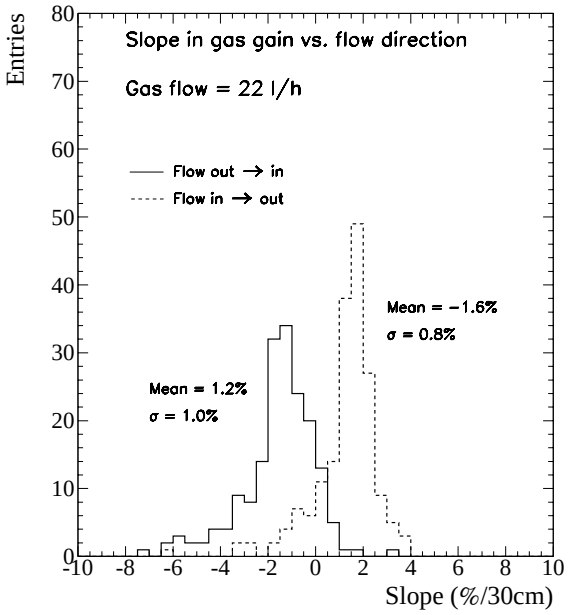

Figure 20: *Slope of gas gain for a flow of* 22 l/h, *for all straws of web 11D (*$\sim$ 180 *straws), and for both gas flow directions.*

This effect was verified when dedicated tests were carried out. An unbiased sample (with respect to straw shape) of 180 straws was tested with a gas flow of 22 l/h for both gas directions. The resulting slope distributions are shown in Fig. 20. (In both cases the slope is calculated towards the centre of the wheel.) It is clear that the slope changes sign from -1.6% to $+1.2\%$, i.e. the slope is inverted following the flow direction. The observed dependence on the gas flow also agrees with the expected behaviour, as shown in App. C.

3.4 Slope-corrected gas gain variation

Gas gain slope due to gas flow has to be accounted for before interpreting gas gain variation in terms of wire offsets. In order to correct the results given by the procedure defined in Section 2.2, two methods are used.

3.4.1 1st method: global correction

The first way incorporates a global correction in the signal amplitude, by subtracting the expected deviation due to the gas flow slope, $\alpha_{\rm flow}$, from each measured amplitude A_i. The average deviation used is $-0.78\%/(30$ cm) (resp. $-1.24\%/(30$ cm)) for a gas flow of 20–22 l/h (resp. 10 l/h). We compute the corrected eccentricity, $(\delta A/A)^{\rm cor}$, as

$$\left(\frac{\delta A}{A}\right)^{\rm cor} \equiv \frac{A^{\rm cor}_{\rm max} - A^{\rm cor}_{\rm min}}{A^{\rm cor}_{\rm avg}}, \tag{2}$$

with

$$A^{\rm cor}_i \equiv A_i[1 - |\alpha_{\rm flow}|(L_3 - L_i)], \qquad i = 1,\, 2,\, 3. \tag{3}$$

The new values for the corrected $(\delta A/A)^{\rm cor}$ parameter per straw are displayed in Figs. 21 and 22. As expected, smaller values for $(\delta A/A)^{\rm cor}$ compared to $\delta A/A$ are found, with an average value of 2.1% instead of 2.4% as quoted in the previous case (Sec. 3.1,

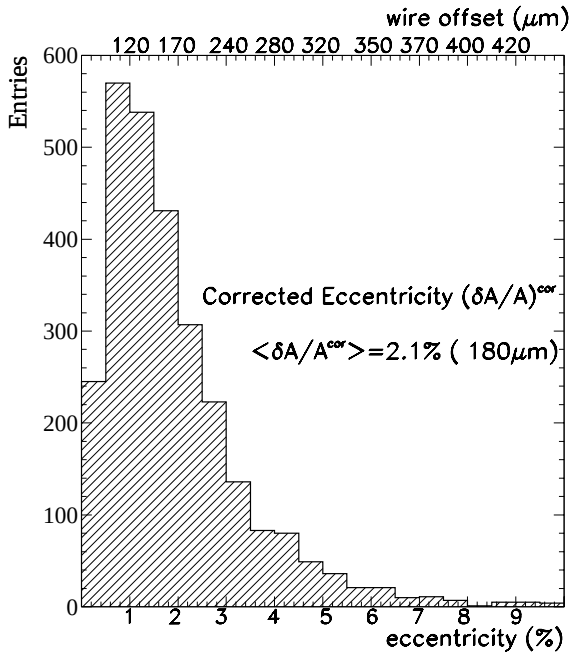

Figure 21: *Maximal gas gain variation for all straws of the wheel after global gas slope correction.*

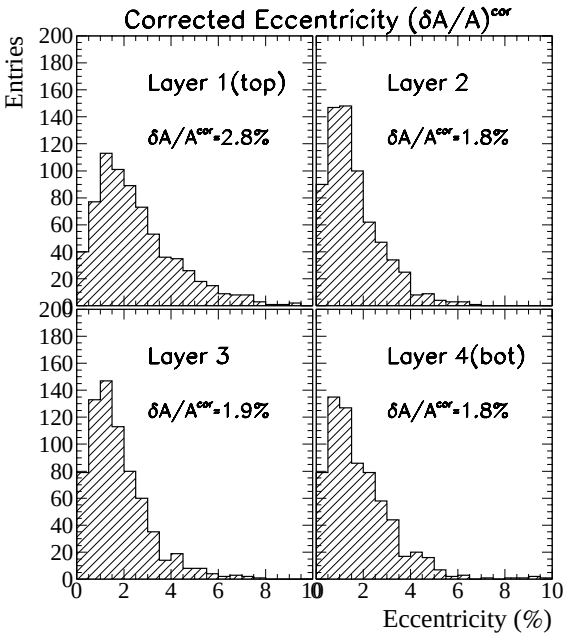

Figure 22: *Maximal gas gain variation for straws of each layer after global gas slope correction.*

Fig. 10). It has to be noted that for a few cases, $(\delta A/A)^{\rm cor}$ increases after the application of the correction, due to the initial shape already displaying a positive-sign slope. These cases are most likely to be explained by a wire incorrectly positioned (off-centre) in the end piece of the straw.

3.4.2 2nd method: individual correction

A second way to account for the gas flow resulting slope is based on a new definition of the eccentricity parameter. We now define $\delta C/C$ as the deviation between the measured and the expected amplitude as seen in the straw centre (position L_2):

$$\frac{\delta C}{C} \equiv \frac{A_2^{\rm meas} - A_2^{\rm exp}}{A_2^{\rm exp}} \tag{4}$$

where $A_2^{\rm meas}$ is the measured signal amplitude and $A_2^{\rm exp}$ the expected amplitude value at this point, computed from the linear fit of the extreme parts signal amplitudes, A_1 and A_3. Notice that this definition assumes that the wire offset is mainly seen in the centre of the straw. It may not be as meaningful for off-centred wires at the straw ends.

Figures 23 and 24 display the parameter for all straws and for each layer separately, respectively. With this definition, an averaged straw eccentricity of 1.3% is found, to be compared to the 2.1% in the previous case. However, an interpretation in terms of wire offset cannot be performed using the curve of Fig. 5. The latter is based on the *maximal* gas gain variation along the straw, which is represented by the $\delta A/A$ parameter, and not on a *relative* variation, as $\delta C/C$ implies. Due to this reason, as well as to the assumption

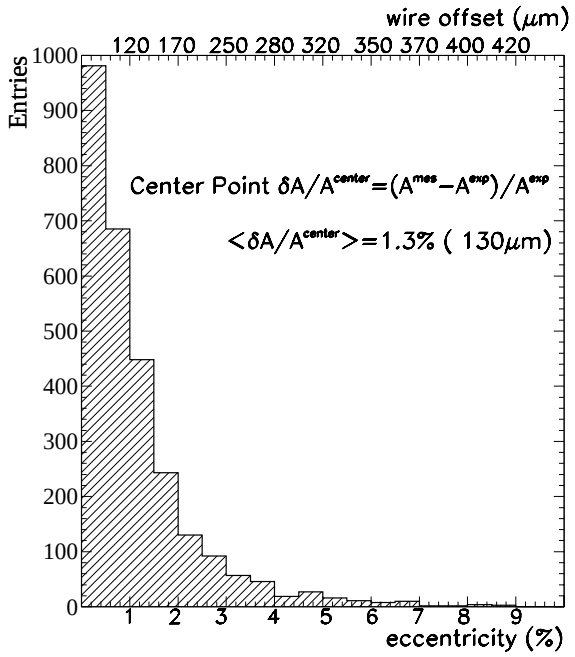

Figure 23: *Maximal gas gain variation for all straws of the wheel after individual gas slope correction.*

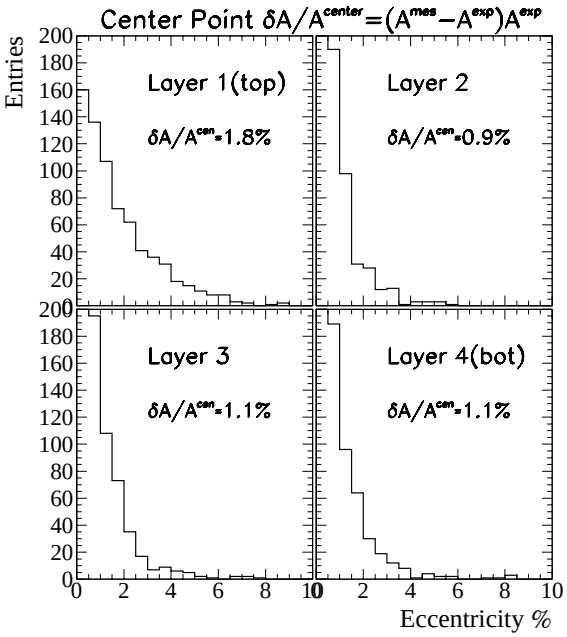

Figure 24: *Maximal gas gain variation for straws of each layer after individual gas slope correction.*

of the location of the maximum amplitude, this way for correcting for the gas slope will not be applied in the following studies.

3.5 Interpretation in terms of wire offset

Once corrected, straw eccentricity measurements can be interpreted in terms of wire offset. This interpretation is provided in Sec. 2.2.2 in the form of an eccentricity-versus-wire-offset plot. As mentioned in the introduction, eccentricity can be either due to off-centered wire in two ends of the straw, or due to the bending of the straw itself. Sagging of the wire has been excluded as a possible reason for non-uniformity of the gas gain along the straw. Relevant measurements, described in Ref. [5], have shown that all wires meet the specifications as far as tension is concerned.

In the following, only values of the corrected eccentricity $(\delta A/A)^{\rm cor}$ are considered. We assume that the remaining gas gain variation is due to a wire offset, deriving the corresponding offset from the eccentricity $\delta A/A$ distributions by using the correspondence given in Fig. 5. Figure 25 displays the straw offset distribution for each individual layer, while a similar distribution for all straws is shown in Fig. 21.

Table 5 provides the distribution of the straws as a function of the eccentricity and the corresponding wire offset. Only 4% straws show an offset above 300 μm; about half of those straws are identified as belonging to layer 1, as expected. About 0.2% (seven straws) of the measured straws have an offset above 400 μm, which can be critical for the safe operation of the detector. In has to be noted, however, that these results have not been corrected for the influence of the environmental conditions change, which may

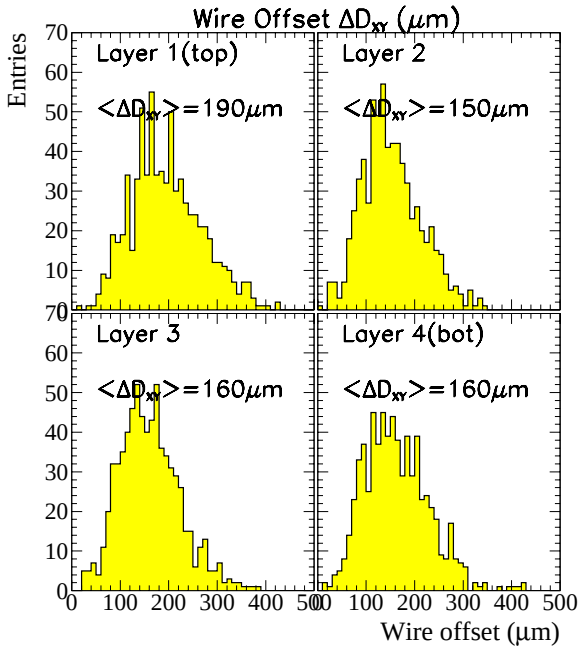

Figure 25: *Amplitude variation interpreted in terms of wire offset. The correspondence of wire offset versus gas gain variation is obtained from Ref. [2].*

Wire offset (μm)	[0, 100)	[100, 200)	[200, 300)	[300, 400)	[400, ∞)
Eccentricity $\delta A/A$ (%)	[0, 0.7)	[0.7, 2.4)	[2.4, 4.8)	[4.8, 8.2)	[8.2, ∞)
Layer 1	8.2%	46.8%	36.1%	8.4%	0.5%
Layer 2	20.0%	58.7%	19.7%	1.6%	0.0%
Layer 3	16.3%	58.5%	22.3%	2.9%	0.0%
Layer 4	18.2%	53.5%	25.9%	1.9%	0.5%
All layers	15.6%	54.3%	26.1%	3.8%	0.2%

Table 5: *Distribution of straws in terms of eccentricity and wire offset for the first 4-plane wheel after correction for the slope due to gas flow. Results are also reported individually for each of the four layers. The percentages are calculated with respect to the number of the actually measured straws.*

increase the gas gain variation. This influence is taken into account when testing the 8-plane wheels using the WTS.

3.6 Effect of wire offset on the energy resolution

It is shown in Ref. [2] that the field distortion generated by a wire offset affects the mean size of the electrons avalanche, thus affecting the signal amplification. The impact of the latter on the observed spectrum is two-fold: the peak position moves to higher values and the spectrum becomes wider and asymmetric. Both effects are seen in Figure 4, where the signal spectrum for straws with various eccentricity values is displayed, as well as in Fig. 17 of Ref. [2]. In this section, we focus on the peak broadening due to the field distortion.

Measurements performed on 34 cells are devoted to the energy resolution study, and

thus also include measurements of the main peak width. Among the 1 088 tested straws, 66 are found dead, leaving 1 022 straws available for analysis. The gas gain variation was calculated as previously, but no correction for the gas slope was applied.

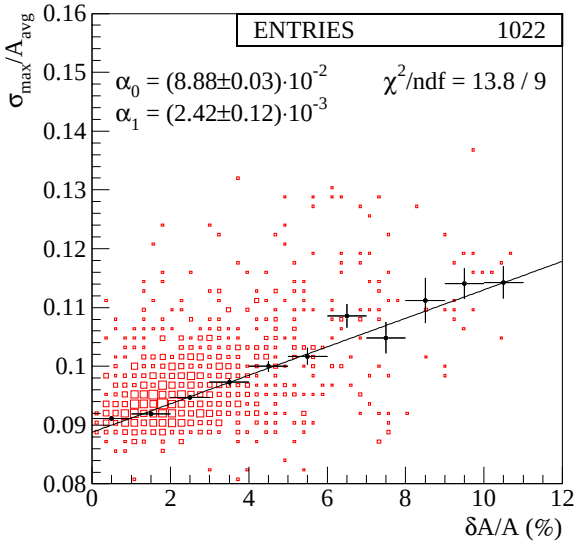

Figure 26: *Normalized maximal signal width $\sigma_{\max}/A_{\text{avg}}$ as a function of measured gas gain variation, $\delta A/A$, for all measured straws. A linear fit, $y = \alpha_0 + \alpha_1 x$, has been applied.*

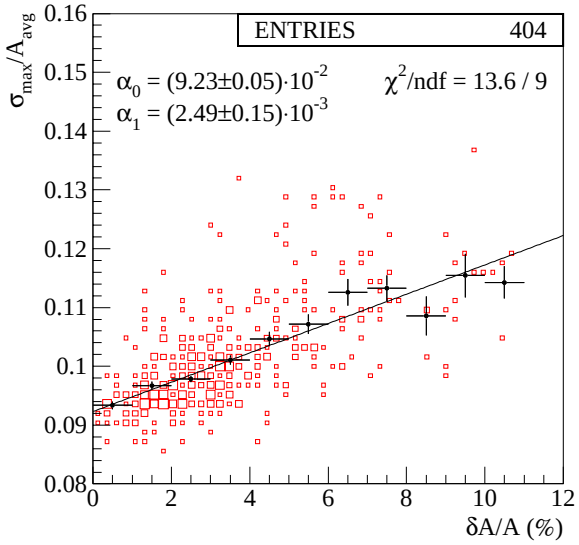

Figure 27: *Normalized maximal signal width $\sigma_{\max}/A_{\text{avg}}$ as a function of measured gas gain variation, $\delta A/A$, for straws with both $A_{\max}$ and $\sigma_{\max}$ at the centre. A linear fit, $y = \alpha_0 + \alpha_1 x$, has been applied.*

Figure 26 shows the normalized (i.e., expressed as a fraction of the mean amplitude, A_{avg}) maximal signal width, $\sigma_{\max}/A_{\text{avg}}$, versus the maximum amplitude variation $\delta A/A$ detected in a straw for all straws. The normalized width is used instead of the absolute, in order to correct for the amplitude change due to factors other than the gas gain. A significant correlation appears between the two variables, although the spread of the measurements is quite large. The same distribution is shown in Fig. 27, for straws demonstrating both the maximum amplitude and width at the centre. The correlation is more pronounced in this plot, since this sample represents more accurately the case of a bent straw. A change in gas gain variation from 3.5% to 5.5% is equivalent to an increase in the signal width of 10%.

It should be mentioned that the width is naively estimated by a Gaussian fit of the peak. Hence, the width value is not that precise for large wire offsets, where the peak appears to be asymmetric. The use of a two-Gaussian fit would provide a more accurate description of the peak broadening and asymmetry.

The variation of the signal width along the straw, $\delta\sigma/\sigma$, versus the measured variation in the peak position, $\delta A/A$, is shown in Fig. 28 for all straws, and in Fig. 29 for straws with $A_{\max}$ and $\sigma_{\max}$ at the centre. A clear trend is seen although the spread is quite large. The width variation seems to be more pronounced than the amplitude variation; a $\delta A/A$ of $\sim 3.5\%$ ($\sim 5.5\%$) corresponds to a $\delta\sigma/\sigma$ of $\sim 9\%$ ($\sim 16\%$).

The wire offset versus width observed correlation is not meant to replace the (more

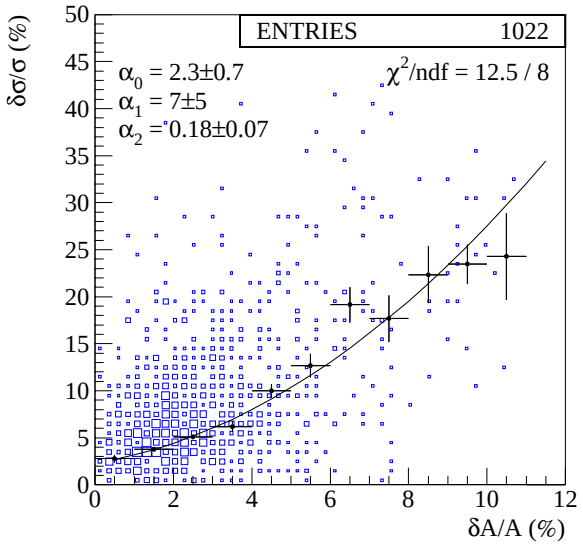

Figure 28: *Variation of the signal width $\delta\sigma/\sigma$ as a function of measured gas gain variation, $\delta A/A$, for all measured straws. A polynomial fit, $y = \alpha_0 + \alpha_1 x + \alpha_2 x^2$, has been applied.*

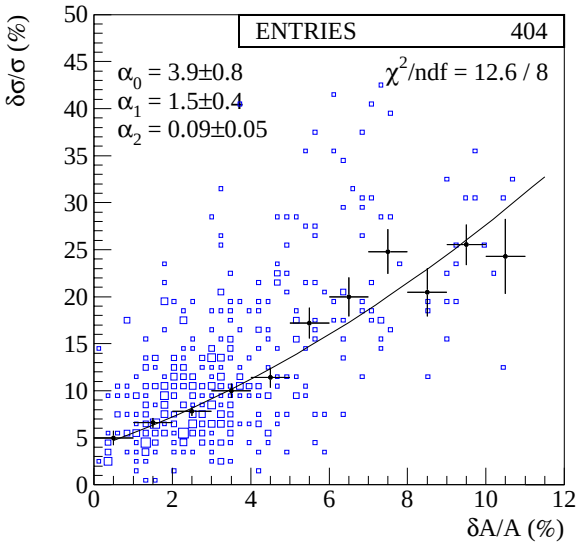

Figure 29: *Variation of the signal width $\delta\sigma/\sigma$ as a function of measured gas gain variation, $\delta A/A$, for straws with both $A_{\max}$ and $\sigma_{\max}$ at the centre. A polynomial fit, $y = \alpha_0 + \alpha_1 x + \alpha_2 x^2$, has been applied.*

accurate) method of gas gain variation. It can be used though as a complementary feature, especially in cases were unusually high amplitude or amplitude variation values are observed. If these variations are due to other factors, such as environmental changes, the corresponding energy resolution should be able to exclude them from being interpreted as due to a wire offset. The asymmetry of the main peak would also be helpful if it could be quantified in terms of, e.g., the skewness, or the comparison between a one-Gaussian and a two-Gaussians fit.

4 Effect of z-deformation

An end-cap TRT is subjected to forces that may deform it in various modes. Here, the aim is to determine the sensitivity of the straws shape in a lateral deformation, through the increased measured eccentricity. Deformation in the z-direction is achieved by applying the necessary force on the inner ring, keeping the outer ring fixed, as shown in Fig. 31. The measurements are repeated for four values of displacement: $\delta z = 0$, 1.5, 2.0, and 3.0 mm. For each of them, 32 straws of cell 1 are scanned in five irradiation points. The five ^{55}Fe-source positions, where measurements of the signal amplitude are performed, are at distances of $d = 13$, 92, 180, 255, and 326 mm from the outer edge of the straw.

The inherent eccentricity values, i.e. obtained with no deformation applied, showed that the sample of straws used are not bent ($\delta A/A < 3\%$). Hence, any further eccentricity measured will be exclusively due to the wheel deformation. The gas gain difference, with respect to point $d_5 = 326$ mm, for each point is shown in Fig. 30. The same results were reviewed on a layer-by-layer basis and no layer-dependent behaviour was observed.

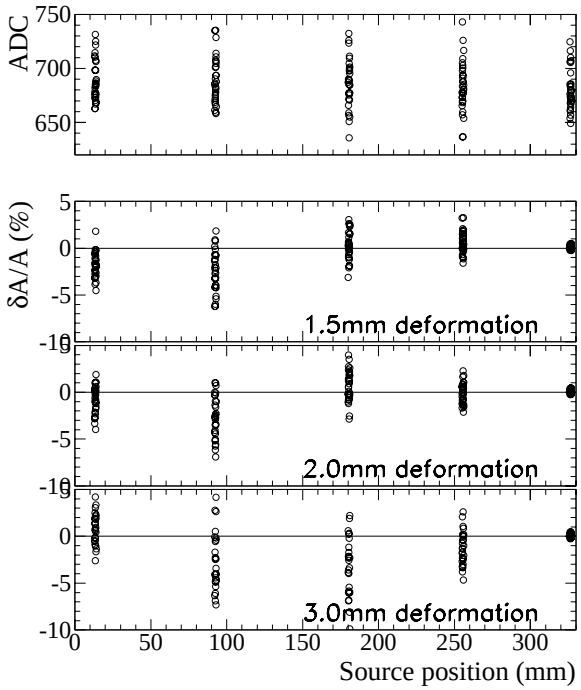

Figure 30: *Amplitude values for each straw at each point without any deformation (top). Divergence of amplitude from inherent value for each point with respect to point* $d_5 = 326\,\mathrm{mm}$ *(bottom). Results for each lateral displacement are presented.*

It is clear from Fig. 30 that a displacement-specific pattern is observed in the straw bending. The expected wire offsets in a 4-plane wheel due to a lateral displacement are calculated in Ref. [6]. According to this study, one should expect the actual straw deformation to be a linear combination of the two modes shown in Fig. 31.

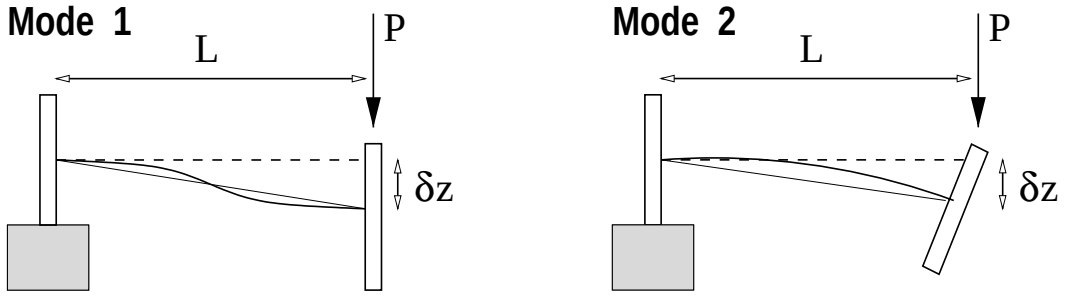

Figure 31: *Lateral force acting on the inner ring. In mode 1 (left), the inner ring is guided and in mode 2 the inner rings moves freely [6]. Only one of the four straw layers is shown.*

An attempt was made to classify each of the $3 \times 32 = 96$ amplitude curves according to this model. The results are shown in Table 6. For a displacement of $\delta z \leq 2\,\mathrm{mm}$, the "S-shape" mode 1 dominates, while for $\delta z \simeq 3\,\mathrm{mm}$, straws are bent following the "U-shape" mode 2. Hence, for low values of δz, the inner ring seems to retain its shape, but for a more intense displacement, the inner ring itself is deformed.

As far as the measured eccentricity is concerned, the maximum effect observed is $\delta A/A \approx 7\%$ (wire offset $\approx 350\,\mu\mathrm{m}$) for $\delta z = 2\,\mathrm{mm}$ and $\delta A/A \approx 10\%$ (wire offset $\approx 440\,\mu\mathrm{m}$) for $\delta z = 3\,\mathrm{mm}$. Since, the maximum eccentricity value accepted is $\approx 5\%$, the wheel should not be deformed during tests or operation more than 2 mm.

Bending modes	Lateral displacement		
	$\delta z = 1.5\,mm$	$\delta z = 2.0\,mm$	$\delta z = 3.0\,mm$
Mode 1	81%	81%	28%
Mode 2	3%	6%	67%
Unclassified	16%	13%	5%

Table 6: *Classification of the 32 scanned straws according to their deformation mode.*

5 Conclusions

The first end-cap TRT 4-plane module was tested systematically with respect to the straw straightness. This has been determined using ^{55}Fe radioactive sources placed at several locations along the straw, where the spectrum is recorded. The method is based on the measurement of the straw eccentricity, defined as the maximal change in the signal amplitude seen along the straw. Several aspects of the straw operation and the measurement procedure itself were understood, besides the direct outcome for the straightness performance of a 4-plane module.

- Many straws were not accessed due to broken traces. The number of straws actually tested (2 820), however, is large enough to allow a comprehensive analysis to be performed.

- In many cases, the straw shape is such that the maximum amplitude is not observed in any of the three points irradiated during this study. More than three source positions will be needed during the mass test of TRT wheels with an automated station in order to obtain an accurate estimation of the wire offset.

- The ϕ-distribution of the eccentricity does not imply any inherent deformation of the first 4-plane wheel, validating, thus, the assembly procedure as far as this aspect is concerned.

- The gas gain decreases by $\sim$1% when moving from the gas inlet to the outlet. This effect, mainly due to oxygen penetration, requires a correction to be applied to the measured eccentricity before interpreting it in terms of wire offset.

- Besides the increase of the signal amplitude, wire offset also results in a degradation of energy resolution and even in a distortion of the spectrum. Hence, recording the standard deviation and/or the skewness of the main peak can provide an additional handle to assess straw straightness.

- According to the ID TDR ([1] p. 659), a safe upper limit for the wire offset is 300 μm. The results obtained from the 4-plane wheel showed that only a fraction of a few percent out of the about 3 000 straws tested are above that limit because of their shape. More specifically, only a few straws per-mille exceed the limit of 400 μm, above which the wires will be disconnected from high voltage.

- A lateral displacement was applied to the wheel. The measured wire offsets showed that the resulting straw deformation becomes critical for a displacement larger than $\sim 2\,\mathrm{mm}$.

The experience acquired by performing a full-scale systematic test of the straw straightness on a 4-plane TRT wheel can be useful while finalizing the design of the Wheel Test Station (WTS). The presented results on the achieved straw straightness can be confirmed and expanded by testing the 8-plane wheel prototype (partly consisted of the first 4-plane module) with the WTS.

Acknowledgements

The authors would like to thank D. Froidevaux, F. Dittus, and A. Romaniouk for useful suggestions in the interpretation of the results. The work of V.A.M. was partially supported by the State Scholarships Foundation of Greece (I.K.Y.).

APPENDICES

A Dead channels

A total of 252 channels showed no response during the testing of the first 4-plane wheel, mainly caused by broken traces on the Kapton layer of the web. Figure 32 displays the location of dead channels for the four layers as a function of the straw index (i.e. ϕ). Dead channels are not distributed uniformly in ϕ. There is also a strong correlation in the concentration of dead channels between layers 2 and 4, which also exhibit a higher number of dead channels when compared with layers 1 and 3. This is due to the location of the traces for layers 2 and 4 in the internal angle of the Kapton board, where traces are more prone to breaking.

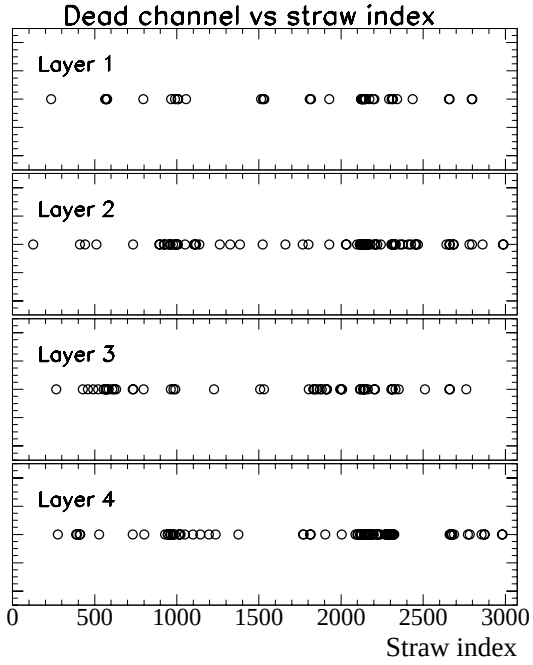

Figure 32: *Location of dead channels versus layer and straw index.*

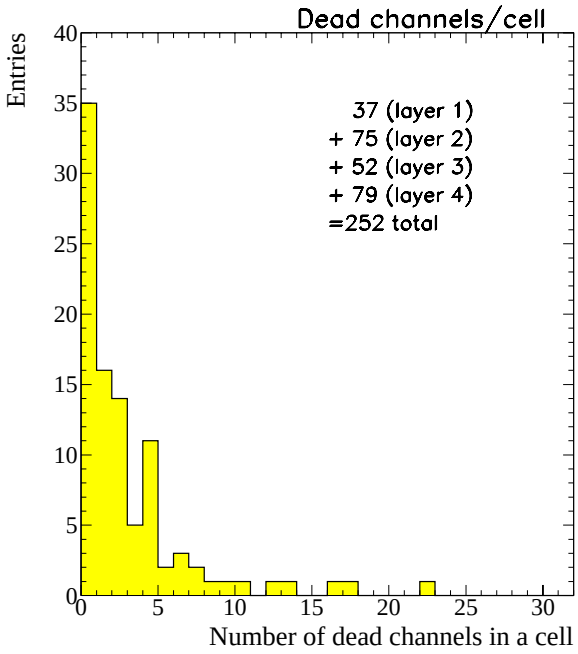

Figure 33: *Number of dead channels per cell for the first 4-plane wheel.*

The non-uniformity of the non-responding in straw index can also be observed in Fig. 33, where the distribution of the number of dead channels per cell is displayed. Those cells (31, 58, 67, 68, 73, 84) with more than 10 dead channels are identified with Kapton FE boards with a lot of visible broken traces. The high number of broken traces for these straws may be due to more tests —hence more manipulations— being carried out on them.

B Cell-to-cell parameter settings

Cell		$< A >$	HV	Flux	Mixture	# dead	Card
#	Web #	ADC	(V)	(l/h)	Ar/CO_2	channels	
1	2A-1	683.7	1428.	22.	1.83	0	B
2	2A-2	655.0	1428.	22.	1.83	0	B
3	2A-3	657.9	1430.	22.	1.83	0	B
4	2A-4	605.9	1401.	22.	1.92	2	B
5	2A-5	518.8	1399.	22.	1.83	0	B
6	2A-6	511.4	1399.	22.	1.83	0	B
7	7B-1	683.1	1400.	20.	2.33	0	A
8	7B-2	716.9	1400.	20.	2.33	1	A
9	7B-3	713.3	1400.	20.	2.33	2	A
10	7B-4	723.9	1400.	20.	2.33	0	A
11	7B-5	445.3	1400.	20.	2.33	0	A
12	7B-6	684.0	1400.	20.	2.33	0	A
13	7A-1	733.0	1430.	22.	2.00	5	B
14	7A-2	733.2	1430.	22.	2.00	2	B
15	7A-3	619.2	1410.	22.	2.00	1	B
16	7A-4	659.3	1421.	22.	2.00	2	B
17	7A-5	667.5	1421.	22.	2.00	2	B
18	7A-6	667.8	1421.	22.	2.00	7	B
19	6C-1	685.8	1421.	22.	2.00	3	B
20	6C-2	666.8	1421.	22.	2.00	2	B
21	6C-3	656.1	1421.	22.	2.00	0	B
22	6C-4	652.5	1421.	22.	2.00	0	B
23	6C-5	659.8	1421.	22.	2.00	4	B
24	6C-6	562.8	1405.	22.	2.00	0	B
25	6B-1	608.1	1415.	22.	1.94	2	B
26	6B-2	603.9	1415.	22.	1.94	1	B
27	6B-3	593.4	1415.	22.	1.94	0	B
28	6B-4	589.8	1415.	22.	1.94	1	B
29	6B-5	587.7	1415.	22.	1.94	4	B
30	6B-6	575.3	1410.	22.	1.94	5	B
31	3A-1	560.8	1410.	22.	1.94	12	B
32	3A-2	557.4	1414.	22.	1.94	8	B
33	3A-3	563.0	1410.	22.	1.94	2	B
34	3A-4	593.2	1414.	22.	1.94	1	B

continued on next page

continued from previous page

Cell		$< A >$	HV	Flux	Mixture	# dead	Card
#	Web #	ADC	(V)	(l/h)	Ar/CO_2	channels	
35	3A-5	591.5	1410.	22.	1.94	4	B
36	3A-6	581.4	1414.	22.	1.94	2	B
37	4C-1	661.1	1400.	20.	2.33	0	A
38	4C-2	697.5	1400.	20.	2.33	1	A
39	4C-3	681.7	1400.	20.	2.33	2	A
40	4C-4	700.6	1400.	20.	2.33	1	A
41	4C-5	427.9	1400.	20.	2.33	0	A
42	4C-6	662.8	1400.	20.	2.33	1	A
43	5C-1	583.3	1410.	22.	1.94	1	B
44	5C-2	587.1	1410.	22.	1.94	1	B
45	5C-3	589.3	1410.	22.	1.94	0	B
46	5C-4	579.8	1410.	22.	1.94	0	B
47	5C-5	583.7	1410.	22.	1.94	0	B
48	5C-6	589.0	1410.	22.	1.94	6	B
49	5B-1	555.1	1410.	22.	1.94	0	B
50	5B-2	547.2	1410.	22.	1.94	0	B
51	5B-3	555.7	1410.	22.	1.94	0	B
52	5B-4	558.4	1410.	22.	1.94	1	B
53	5B-5	565.3	1410.	22.	1.94	0	B
54	5B-6	578.2	1410.	22.	1.94	1	B
55	5A-1	712.1	1400.	20.	2.33	0	A
56	5A-2	763.7	1400.	20.	2.33	3	A
57	5A-3	719.1	1400.	20.	2.33	6	A
58	5A-4	621.0	1400.	20.	2.33	10	A
59	5A-5	445.4	1400.	20.	2.33	2	A
60	5A-6	701.3	1400.	20.	2.33	4	A
61	4D-1	669.4	1400.	20.	2.33	2	A
62	4D-2	712.5	1400.	20.	2.33	0	A
63	4D-3	697.7	1400.	20.	2.33	4	A
64	4D-4	715.9	1400.	20.	2.33	2	A
65	4D-5	438.8	1400.	20.	2.33	0	A
66	4D-6	660.6	1400.	20.	2.33	4	A
67	3D-1	652.4	1400.	10.	2.33	22	B

continued on next page

continued from previous page

Cell		$< A >$	HV	Flux	Mixture	# dead	Card
#	Web #	ADC	(V)	(l/h)	Ar/CO_2	channels	
68	3D-2	653.0	1400.	10.	2.33	16	B
69	3D-3	652.0	1400.	10.	2.33	9	B
70	3D-4	664.8	1400.	10.	2.33	6	B
71	3D-5	664.7	1400.	10.	2.33	2	B
72	3D-6	668.7	1400.	10.	2.33	7	B
73	3C-1	683.4	1400.	10.	2.33	17	B
74	3C-2	764.3	1400.	10.	2.33	3	B
75	3C-3	766.3	1400.	10.	2.33	1	B
76	3C-4	727.9	1400.	10.	2.33	4	B
77	3C-5	637.0	1330.	10.	2.33	3	B
78	3C-6	668.9	1400.	10.	2.33	1	B
79	3B-1	664.8	1400.	10.	2.33	1	B
80	3B-2	664.9	1400.	10.	2.33	0	B
81	3B-3	660.2	1400.	10.	2.33	0	B
82	3B-4	661.6	1400.	10.	2.33	0	B
83	3B-5	656.1	1330.	10.	2.33	1	B
84	3B-6	659.5	1330.	10.	2.33	13	B
85	2D-1	660.5	1400.	20.	2.33	0	A
86	2D-2	712.0	1400.	20.	2.33	0	A
87	2D-3	707.5	1400.	20.	2.33	4	A
88	2D-4	716.3	1400.	20.	2.33	3	A
89	2D-5	437.9	1400.	20.	2.33	0	A
90	2D-6	667.6	1400.	20.	2.33	4	A
91	2B-1	659.6	1330.	40.	2.33	0	B
92	2B-2	660.4	1330.	40.	2.33	0	B
93	2B-3	652.7	1330.	40.	2.33	0	B
94	2B-4	656.9	1330.	40.	2.33	4	B
95	2B-5	650.8	1330.	40.	2.33	0	B
96	2B-6	644.5	1330.	40.	2.33	4	B

C Gas gain variation due to electron attachment to oxygen

As mentioned in Sec. 3.3, the straw walls are permeable to CO_2 and O_2 molecules. Although the escaping CO_2 results in an amplitude increase, the net effect is the decrease of the gas gain due to electron attachment to oxygen. The contamination in oxygen along the straw will be calculated, followed by the estimation of the resulting gas gain loss.

The oxygen molecules penetrate the straw walls according to Darcy's law, which describes the flow of fluids in porous media:

$$\nabla p = -k\mathbf{v} \tag{5}$$

where $\mathbf{v}$ is the velocity of the gas penetrating the medium, p is its pressure in the medium and k is the permeability. The permeability is a constant for slightly porous media as the straw walls. Equation (5) for the straw walls becomes

$$v_r = -\frac{1}{k}\frac{\partial p}{\partial r}, \tag{6}$$

in cylindrical coordinates, where p is the partial pressure of oxygen.

According to the state equation for perfect gases, the partial pressure of oxygen is

$$p = \rho\frac{\Lambda}{M}T, \tag{7}$$

where ρ and M are the density and molecular weight of oxygen, respectively, $\Lambda = 8314\,\mathrm{m^2/(s^2K)}$ is a universal constant, and $T = 293\,\mathrm{K}$ is the temperature (the procedure is assumed isothermal). Assuming that v_r is constant in the straw wall, the gradient of pressure is

$$\frac{\partial p}{\partial r} \simeq \frac{\rho_0 - \rho(z)}{b}\frac{\Lambda}{M}T, \tag{8}$$

where $\rho_0 = \text{const.}$ and $\rho(z)$ are the oxygen densities outside and inside the straw, respectively, and b is the straw wall thickness. Hence, Eqs. (6) and (8) give

$$v_r = -\frac{\Lambda T}{kbM}[\rho_0 - \rho(z)] \tag{9}$$

Let a infinitesimal volume of length Δz of the straw. We assume that ρ and v_z are constant in the $r\phi$-plane, i.e., they only vary with z. Then, the inflow per time unit (the flow is steady), Q_{in}, is

$$Q_{\mathrm{in}} = \rho(z)v_z(z)\pi R^2 + \rho(z)|v_r|\,2\pi R\,\Delta z, \tag{10}$$

where R is the straw radius. The outflow, Q_{out}, is

$$Q_{\mathrm{out}} = \rho(z)v_z(z)\pi R^2 + \frac{\mathrm{d}(\rho v_z)}{\mathrm{d}z}\,\Delta z\,\pi R^2. \tag{11}$$

By equating $Q_{\rm in} = Q_{\rm out}$, Eqs. (10) and (11) give

$$\frac{\mathrm{d}(\rho v_z)}{\mathrm{d}z} = \frac{2\Lambda T}{kbMR}\,\rho(\rho_0 - \rho). \tag{12}$$

The flow velocity along the z-direction does not change as rapidly as the density, so it can be considered constant, $v_z = V$, thus Eq. (12) becomes

$$\frac{\mathrm{d}\rho}{\mathrm{d}z} = \lambda\rho(\rho_0 - \rho), \qquad \text{with} \qquad \lambda \equiv \frac{2\Lambda T}{kVbRM}. \tag{13}$$

By applying the initial condition $\rho = \alpha\rho_0$ ($\alpha < 1$) at $z = 0$, the differential Eq. (13) gives

$$\int_{\alpha\rho_0}^{\rho} \frac{\mathrm{d}\rho}{\rho(\rho_0 - \rho)} = \lambda \int_0^z \mathrm{d}z \quad \Longrightarrow \quad \int_{\alpha\rho_0}^{\rho} \frac{\mathrm{d}\rho}{\rho} + \int_{\alpha\rho_0}^{\rho} \frac{\mathrm{d}\rho}{\rho_0 - \rho} = \lambda z$$

$$\Longrightarrow \quad \ln\left(\frac{\rho}{\alpha\rho_0}\right) - \ln\left(\frac{\rho_0 - \rho}{\rho_0 - \alpha\rho_0}\right) = \lambda z \quad \Longrightarrow \quad \rho(z) = \rho_0 \frac{\alpha e^{\lambda z}}{1 + \alpha(e^{\lambda z} - 1)}, \tag{14}$$

which expresses the oxygen contamination along the straw.

Now, the effect of oxygen presence on the gas gain will be calculated. The number of free electrons in an oxygen-contaminated gas follows the law [7]

$$N(t) = N_0 e^{-At} \tag{15}$$

where N_0 is the number of free electron at $t = 0$. The attachment rate, A, can be factorized as

$$A = C_{O_2,M} \cdot p_M \cdot p_{O_2}, \tag{16}$$

where p_M and p_{O_2} are the partial pressures of the gas mixture M ($\mathrm{Ar/CO_2}$ in our case) and the oxygen, respectively, and $C_{O_2,M}$ is the attachment coefficient.

Since $p_{O_2} = \beta p_M$, where β is the contamination in oxygen, $A = C_{O_2,M} \cdot p_M^2 \cdot \beta$. For the mixture used, $p_M \simeq 10^5\,\mathrm{Pa}$ and a typical value of the attachment coefficient for an argon-based mixture is $C_{O_2,M} \approx 3 \cdot 10^{-9}\,\mu\mathrm{s}^{-1}\mathrm{Pa}^{-2}$ [7]. Using typical values of the drift velocity ($v_{\rm drift} \simeq 5 \cdot 10^4\,\mathrm{m/s}$ from Ref. [1] p. 616) and the distance between the track and the wire ($d \approx 1\,\mathrm{mm}$), the drift time is calculated to be $t \approx 20\,\mathrm{ns}$. By substituting the previous values in Eq. (16), we get $At = 0.6\beta$. Equations. (15) and (16), give the ratio R of the collected charge Q over the charge Q_0 initiated by the particle passage:

$$R(\beta) = \frac{Q(\beta)}{Q_0} = \frac{N(\beta)}{N_0} = \exp\left(-C_{O_2,M} \cdot p_M^2 \frac{d}{v_{\rm drift}}\,\beta\right). \tag{17}$$

The contamination parameter β is related to the oxygen density by the equation

$$\beta = \frac{\rho(z)}{\rho_M} = \frac{\rho_0}{\rho_M}\left(\frac{\rho(z)}{\rho_0}\right), \tag{18}$$

where $\rho_M = 1.7\,\mathrm{kg/m^3}$ is the density of $70\%\mathrm{Ar} + 30\%\mathrm{CO_2}$ mixture and $\rho_0 = 0.27\,\mathrm{kg/m^3}$.

By combining Eqs (14), (17), and (18), we get the fractional gas gain loss, R, due to oxygen penetration into the straw, as a function of the distance along the straw, z:

$$R(\beta) = \exp\left[-B\frac{\alpha e^{\lambda z}}{1+\alpha(e^{\lambda z}-1)}\right], \quad \text{where} \quad B \equiv C_{O_2,M}\cdot p_M^2 \frac{d}{v_{\text{drift}}}\frac{\rho_0}{\rho_M}. \tag{19}$$

By substituting the previous approximate values for the relevant parameters of coefficient B, we get a rather indicative value for it: $B \approx 0.1$.

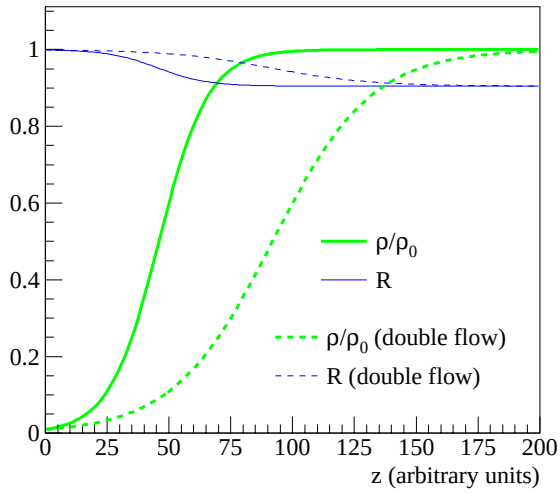

Figure 34: *Oxygen density (thick, green) and gas gain ratio (thin, blue) for $\lambda = 0.1$ (full line) and $\lambda = 0.05$ (dashed line); the latter corresponding to a double gas flow. The coefficients $\alpha = 0.01$ and $B = 0.1$ have been used.*

Figure 34 illustrates the relative oxygen density ρ/ρ_0 and the corresponding gas gain ratio R, as functions of the distance along the straw, z (in arbitrary units). At $z = 0$, oxygen penetration is assumed to be at the level of 1% ($\alpha = 0.01$). A typical value corresponding to our setup of $B = 0.1$ is also assumed.

The gas gain drops rapidly as the oxygen density rises. For $z \to \infty$, the oxygen density ρ becomes equal to the atmospheric one, ρ_0, as it reaches equilibrium. In this limit, the relative gas gain tends to be equal to $e^{-\beta} \simeq 0.9$, which is consistent with the one observed (Sec. 3.3) in our setup. Moreover, after a certain distance the gas gain should be stable as the effect reaches saturation.

In order to understand the dependence of this effect on the value of gas flow, two values for λ are used: 0.1 (continuous) and 0.05 (dashed) in arbitrary units. Since $\lambda \propto 1/V$, the second value corresponds to a gas flow twice as high as the first one. It is clear from Fig. 34 that the slope becomes less apparent when the gas flow is increased, but it takes a longer straw length to reach equilibrium. This is consistent with the observed slopes for different gas flows presented in Sec. 3.3.

References

[1] ATLAS Collaboration, Inner Detector Technical Design Report, vol. II, CERN/LHCC/97-17 (1997).

[2] P. Cwetanski, A. Romaniouk, and V. Sosnovtsev, "Studies of wire offset effects on gas gain in the ATLAS TRT straw chamber", ATLAS Internal Note ATL-INDET-2000-016 (2000).

[3] E. David *et al.*, "Test of the TRT end-cap wheel", ATLAS Internal Note ATL-INDET-97-169 (1997).

[4] O. Fedin *et al.*, "A measurement station for the ATLAS end-cap TRT calibration", ATLAS Communication ATL-COM-INDET-99-026 (1999);
N.V. Klopov *et al.*, "Testing and data storage of TRT end-cap wheels", ATLAS Project Document ATL-IT-TP-0005 (2001).

[5] E. Barberio *et al.*, "Wire tension measurements for the ATLAS end-cap TRT", ATLAS Internal Note ATL-INDET-2000-003 (2000).

[6] H. Danielsson, "Wire offset in a 4-plane module under a lateral force", Technical Note CERN/TA1/00-02 (2000).

[7] M. Huk, P. Igo-Kemenes, and A. Wagner, "Electron attachment to oxygen, water, and methanol, in various drift chamber gas mixtures", HD-PY 87/12 (1987).